Insert-Molded Poly(ether imide)/Carbon Fiber Poly(ether ether ketone) Bimaterial Composites: Fracture and Interfacial Analysis

Sung In Moon, L. L. Monson, C. W. Extrand

Entegris, 3500 Lyman Blvd., Chaska, Minnesota 55318

Received 6 February 2006; accepted 18 March 2006
DOI 10.1002/app.24483
Published online in Wiley InterScience (www.interscience.wiley.com).

ABSTRACT: Bimaterial composites were constructed by injecting carbon-fiber-filled poly(etheretherketone) (CF PEEK) into a mold containing one-half of a poly(etherimide) (PEI) tensile specimen. Specimens were notched at the interface and tested in tension. Using fracture mechanics, the adhesion strength of the interface (a fracture energy with units of energy per area) was calculated from notch size and stress–strain behavior of the notched specimens. Fracture energies (with units of energy per area) of the PEI/CF PEEK bimaterial composites were slightly less than those measured from the monolithic materials of construction. Variations in test speed (below the glass transition temperature of the two components) had little effect on stiffness or fracture energy. However, fracture energies decreased slightly as temperature increased. Composites fractured through the CF PEEK near the PEI/CF PEEK interface. Consequently, the fracture surface of the PEI portion had a thin layer of CF PEEK (a qualitative indicator of good adhesion). Microscopy and X-ray photoelectron spectroscopy confirmed the presence of a thin layer of CF PEEK on the PEI. It appears that the miscibility of PEI and PEEK contributed to the strength of the PEI/CF PEEK thermophysical bond. The strength of the thermophysical bond of the PEI/CF PEEK bimaterial composites was greater than the cohesive strength of amorphous commodity polymers such as polystyrene and should be more than adequate for most microelectronics device handling applications. J Appl Polym Sci 102: 2362–2371, 2006

Key words: injection molding; composites; fracture; mechanical properties; high performance polymers

INTRODUCTION

Insert-molding often involves molding a higher performance polymer, such as poly(etheretherketone) (PEEK), on to a less expensive one. This approach combines the best features of both materials and provides an economical method of producing higher performance products at a reduced cost.[1,2] In some cases, it is a good alternative to polymer blends.

Recently, insert-molding has been employed in the construction of poly(carbonate) (PC)/carbon fiber polyetheretherketone (CF PEEK) containers for the transportation and storage of silicon wafers.[3–7] While PC is clean, tough, and dimensionally stable, among engineering polymers, it has modest chemical and thermal resistance. Therefore, it would be desirable to pair PEEK with a material that has greater chemical and thermal resistance. An excellent candidate for higher performance is polyetherimide (PEI). PEI, like PC, is a rigid, amorphous polymer that has several advantages over PC, such as greater stiffness, better chemical resistance, a higher glass–rubber transition temperature,[8–10] and better flame retardancy. Also, PEI is miscible with PEEK,[11–15] which potentially could lead to improved adhesion. These properties make PEI an attractive alternative to PC where higher performance bimaterial composites are required.

One of the key features of any successful product based on insert-molding is good adhesion between the materials. Thus, the purpose of this study was to evaluate the adhesion between PEI and CF PEEK. Composite samples were constructed by injecting CF PEEK into a mold containing one-half of a PEI sample. The interface acts as a flaw or stress riser of unknown size. To perform a controlled measurement, notches of predetermined size were intentionally introduced into specimens prior to testing. Notched samples were tested in tension. Using fracture mechanics, the adhesion strength of the interfaces was calculated from notch size and stress–strain behavior of the notched specimens. Effect of notch size, test speed, and temperature were examined for the composite as well as the materials of construction (PEI and CF PEEK). Also, fracture surfaces were analyzed using optical microscopy (OM), scanning electron microscopy (SEM), and X-ray photoelectron spectroscopy (XPS).

Correspondence to: C. W. Extrand (chuck_extrand@entegris.com).

ANALYSIS

Crystallinity

The crystalline fraction x_c of the CF PEEK was calculated as[16]

$$x_c = (\Delta H/H_f)/(1 - x_f), \quad (1)$$

where x_f is the filler fraction, ΔH is the measured melting enthalpy, and H_f is the melting enthalpy of the polymer in a 100% crystalline state. For PEEK, $H_f = 130$ J/g.[17]

General mechanics

Tensile stresses σ were calculated using elongation force F divided by the undeformed cross-sectional area A,[18,19]

$$\sigma = F/A. \quad (2)$$

Tensile strains ε were calculated using elongation ΔL of the sample divided by its initial length L,

$$\varepsilon = \Delta L/L. \quad (3)$$

Tensile moduli E were calculated as stress σ over strain ε, where strains were small and the materials were linearly elastic ($\varepsilon < 0.01$),

$$E = \sigma/\varepsilon. \quad (4)$$

Strain rate $\hat{e}$ was calculated as the velocity v of the elongation divided by the initial length L,

$$\hat{e} = v/L. \quad (5)$$

Mechanics of composite specimens

Figure 1(a) shows the central portion of a bimaterial composite tensile specimen. The specimen is composed of two materials in series with tensile moduli of E_1 and E_2, where $E_1 \leq E_2$. Both segments have the same cross-sectional area, A, but the relative length of each component, L_1 and L_2, can vary.[4,7] When load is applied, the bimaterial composite deforms with the same average stress in each component, independent of fractional length,

$$\sigma = \sigma_1 = \sigma_2. \quad (6)$$

However, if the materials of construction differ in their stiffness, the individual components will not deform to the same extent. The stiffer material deforms less, while the softer material deforms more. The apparent strain, ε, in the composite sample is the sum of the strain in each of the components,

$$\varepsilon = \Delta L/L = \lambda_1\varepsilon_1 + (1 - \lambda_1)\varepsilon_2, \quad (7)$$

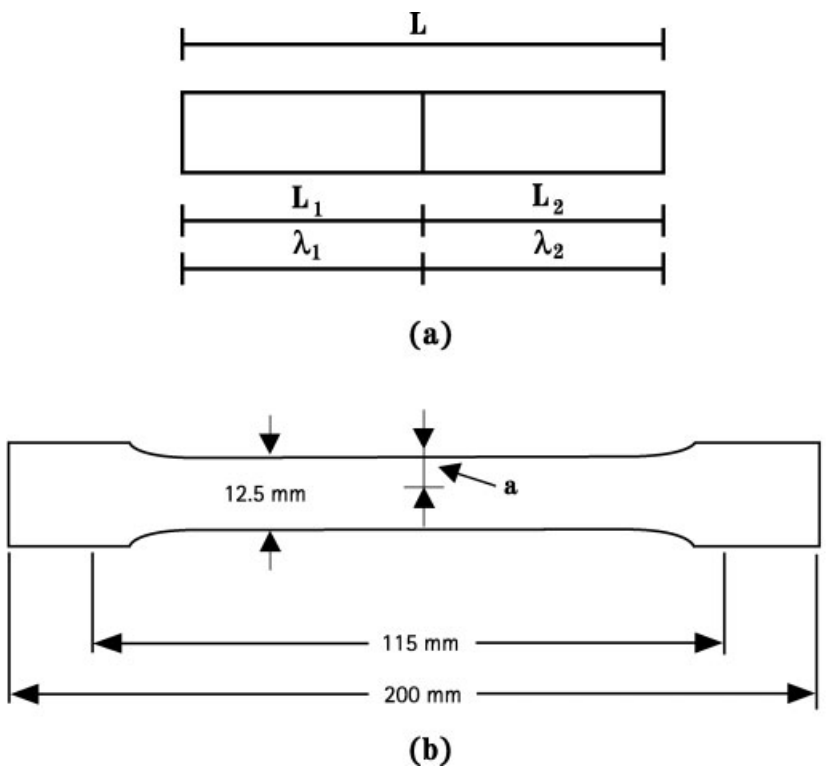

Figure 1 (a) The central portion of a series composite tensile specimen composed of two materials with different tensile moduli, E_1 and E_2, where $E_1 < E_2$. In all cases reported here, $\lambda_1 = \lambda_2 = 0.5$. (b) The dimensions of the whole tensile specimen as well as notch location and orientation. The notch length a was zero for unnotched samples.

where

$$\lambda_1 = L_1/L, \tag{8}$$

$$\lambda_2 = L_2/L, \tag{9}$$

$$\varepsilon_1 = \Delta L_1/L_1, \tag{10}$$

$$\varepsilon_2 = \Delta L_2/L_2, \tag{11}$$

and

$$\lambda_1 + \lambda_2 = 1. \tag{12}$$

Thus, the apparent stress generated within a bimaterial composite specimen depends on the applied apparent strain, component moduli, and component fractional lengths,

$$\sigma = E_1E_2/[\lambda_1E_2 + (1 - \lambda_1)E_1]\varepsilon. \tag{13}$$

Accordingly, the apparent tensile modulus, E, of the bimaterial composites is

$$E = E_1E_2/[\lambda_1E_2 + (1 - \lambda_1)E_1]. \tag{14}$$

For all specimens examined in this study, $\lambda_1 = \lambda_2 = 0.5$.

Fracture mechanics

The adhesive strength of the interface and the component materials were calculated using fracture mechanics. The fracture energies G were calculated from the notch length a and mechanical response of notched specimens as[20,21]

$$G = 2.5\ \pi aU, \tag{15}$$

where U is the strain energy density to break (or area under the stress–strain curve). U is computed by integrating the stress–strain curve from $\varepsilon = 0$ to $\varepsilon = \varepsilon_b$,

$$U = \sigma(\varepsilon)\ d\varepsilon. \tag{16}$$

If specimens broke at small strains with a linear stress–strain response, approximate values of fracture energy were estimated from breaking stresses and strains as,

$$G^* = 1.25\ \pi a\sigma_b\varepsilon_b \tag{17}$$

or simply from the breaking stress,

$$G^{**} = 1.25\ \pi a{\sigma_b}^2/E. \tag{18}$$

EXPERIMENTAL

Materials

PEI (Ultem 1000 from GE, Pittsfield, MA) and CF PEEK (Entegris' STAT-PRO® 300E, Chaska, MN) were used to mold monolithic and bimaterial composite specimens. The PEI had $M_n \approx 1.2 \times 10^4$ g/mol and a polydispersity, Z, of 1.9. The CF PEEK compound contained $< 20\%$ short carbon fiber ($M_n \approx 3.1 \times 10^4$ g/mol with $Z \sim 2.4$).

Sample preparation

Figure 1(b) shows typical dimensions of ASTM D638 Type I tensile specimen. Monolithic tensile specimens were molded from the individual resins by injection molding. Composite samples were fabricated by first molding PEI specimens, then cutting them in half with a bandsaw, and inserting the half pieces back into the mold. CF PEEK was then injected into the mold containing the half piece of PEI. In all cases, $\lambda_1 = \lambda_2 = 0.5$.

Tensile specimens were notched at their midpoint. For the composite specimens, this corresponded to placing the notch at the interface. Figure 1(b) shows the notch orientation. First, a Ryobi® SC165VS scroll saw with a 0.025″ (0.64 mm) coarse tooth blade at $\sim$ 900 strokes per minute was used to cut within 0.5 mm (0.02″) of the desired depth. Then, a Master Mechanic® universal style utility blade was mounted in the INSTRON® 5582 test machine to cut the final 0.5 mm. A specimen was placed in the tensile tester and the blade was brought into contact with the edge near the notch. A pressure reading of less than 1 N was used to signify contact and then the gauge length was reset. After resetting gauge length and centering the partially cut notch under the blade, the machine was started. The blade moved downward at 2 mm/min until the preprogrammed notch length was reached. Notch length a was varied between 1 and 4 mm.

Melt flow rate

Melt flow rate (MFR) was determined using a Kayeness Galaxy I melt flow indexer with a 1.048 mm orifice. Triplicate samples were cut from tensile specimens and dried for 4 h at 150°C. Six grams of material was loaded into the instrument. Barrel temperatures were 337°C for PEI and 385°C for CF PEEK. After preheating for 6 min, a 6.6 kg load was applied to the PEI and 5.0 kg load to CF PEEK (ASTM D1238-98). MFRs were reported in dg/min.

Differential scanning calorimetry

Glass transition temperatures, T_g, and melting temperatures, T_m, were determined using a Perkin–Elmer DSC7 differential scanning calorimeter (DSC). Three samples, with masses of 4–7 mg, were taken from tensile bars and scanned at a rate of 10°C/min. For PEI, samples were heated from 20 to 300°C, cooled to 20°C, and then heated a second time to 300°C. For CF PEEK, samples were heated to 400°C, cooled to 20°C, and

then heated again to 400°C. Analysis was performed using the software resident in the DSC7. T_g values were taken from inflection point of the second heating run. Melting properties of CF PEEK were taken from the peak of the first heating run to reflect cystallinity after molding.

Mechanical testing

Samples were tested in tension using an INSTRON® 5582 test machine equipped with a 100 kN static load cell and extensometer (ASTM D638). Most samples were elongated at 2 mm/min and 23°C. Alternatively, some were tested at other speeds or temperatures to examine any potential rate or temperature effects. Five samples of each type were tested for yield stress, yield strain, breaking stress, breaking strain. Moduli and strain energy densities were determined from stress–strain curves. For notched samples, notch size, breaking stresses, breaking strains, moduli, and strain energy densities were used to calculate fracture energies. Averages and standard deviations were calculated for each specimen type tested.

Microscopy

The fracture interfaces of the bimaterial composites were investigated using both optical microscopy (OM) and scanning electron microscopy (SEM). For OM, thin slices were cut from the interfacial regions to improve the transmittance of light, and images were captured using a Nikon SMZ1500 microscopy with magnifications as high as 100×. However, at 100×, the depth of focus became too shallow to clearly distinguish surface features. To obtain higher magnification, the fracture surfaces were coated with a 5 nm layer of platinum prior to SEM imaging at 200× with a Jeol 6500. (Magnifications greater than 200× severely limited the viewable area and were not used in this study.)

X-ray photoelectron spectroscopy

X-ray photoelectron spectroscopy (XPS) spectra were obtained using a Quantum 2000 instrument (Physical Electronics). A monochromatic Al Kα line was used for excitation source. All the spectra were taken using a 45° take-off angle (the angle between the sample surface and the detector).

RESULTS AND DISCUSSION

Flow and thermal properties

Table I shows the flow and thermal characteristics of the materials used in both the monolithic specimens and the composites. MFR from the molded specimens of the CF PEEK and PEI fell within manufacturers' specifications and were unchanged compared to values measured for the resin, suggesting that no degradation occurred during molding. Thermal properties of the various monolithic and bimaterial were in general agreement with literature values.[12–16] Amorphous PEI had a glass transition temperature, T_g, of about 220°C. On the other hand, the partially crystalline CF PEEK had a glass transition temperature, T_g, around 145°C and a melt temperature, T_m, of 348°C. The crystalline fraction, x_c, in the CF PEEK was ~35%, which is the maximum attainable crystallinity for PEEK under typical injection molding conditions.

Unnotched samples

Stress–strain behaviors

Figure 2 shows the stress–strain behaviors of a typical PEI/CF PEEK bimaterial composite at room temperature ($\lambda_1 = \lambda_2 = 0.5$, $v = 2$ mm/min). The curve for monolithic CF PEEK and the initial portion of a PEI curve are presented together for comparison. PEI/CF PEEK composites broke without yielding at lower strains than those from the monolithic CF PEEK specimens and their breaking stresses were much lower. Table II summarizes the mechanical properties at room temperature. Properties for the monolithic specimens are in general agreement with literature values.[8,9,12,22–24] The CF PEEK specimens were approximately four times stiffer than the PEI specimens. This means that at room temperature, the PEI portion of the bimaterial specimen experiences 4× the strain of the CF PEEK portion.

Figure 3 shows the relation between tensile modulus, E, and temperature, T, for monolithic PEI, monolithic CF PEEK, and the PEI/CF PEEK bimaterial composites ($\lambda_1 = \lambda_2 = 0.5$). There was little change

TABLE I
Summary of Materials Characterization

Materials	MFR (dg/min)	T_g (°C)	T_m (°C)	ΔH (J/g)	x_c (%)
PEI	8.8 ± 0.3	219 ± 1	NA	0	0
CF PEEK	39.8 ± 0.6	149 ± 3	346 ± 1	40.9 ± 2.7	38 ± 3
PEI from PEI/CF PEEK	10.9 ± 0.2	220 ± 1	NA	0	0
CF PEEK from PEI/CF PEEK	42.6 ± 0.7	146 ± 1	345 ± 1	35.6 ± 1.9	33 ± 2

MFR, melt flow rate; T_g, glass-transition temperature; T_m, melt temperature; ΔH, melt enthalpy; x_c, crystalline fraction; NA, not applicable.

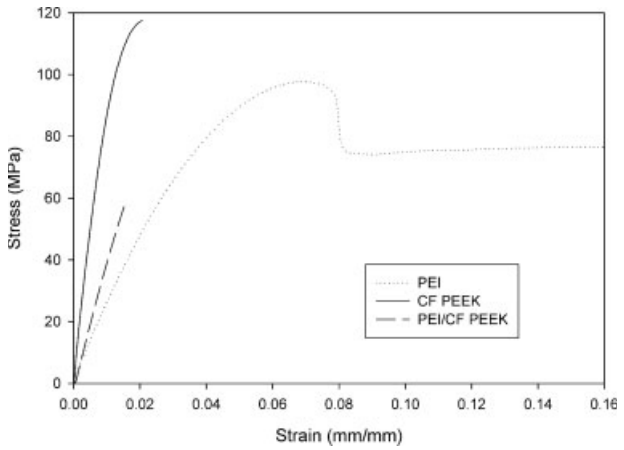

Figure 2 Stress versus strain curves for unnotched bimaterials ($T = 23°C$, $v = 2$ mm/min).

in stiffness of the materials of construction until temperatures reached their respective glass transition temperatures, $T_g = 220°C$ for PEI and $T_g = 145°C$ for PEEK. However, there was a slight dip in the moduli of both PEI and CF PEEK due to secondary thermal transitions in the vicinity of 50–75°C for PEI and 25–50°C for CF PEEK.[23] Above 220°C, the amorphous PEI was a viscous liquid, completely void of structural integrity. On the other hand, the partially crystalline CF PEEK maintained some of its rigidity up to its melting temperature, $T_m = 345°C$.

The stiffness of the PEI/CF PEEK composites was determined to a large degree by the thermal characteristics of the PEI. The stiffness of the PEI/CF PEEK composites declined only slightly with increasing temperature up to the T_g of PEEK. Above 145°C, the PEEK matrix softened and the stiffness of PEI and CF PEEK was nearly identical. With further increases in temperature, the PEI/CF PEEK composites follow the path of PEI. Moduli calculated from eq. (14) agreed well with measured values for all composites. More details regarding the mechanical properties of the PEI/CF PEEK bimaterials can be found elsewhere.[25]

Notched samples

Stress–strain behavior

Figure 4 shows stress–strain behavior of CF PEEK with a 2 mm notch at room temperature. Stress increased linearly with strain, falling off slightly before breaking. No yielding was observed; all the breaks were abrupt and on several occasions, fragments were ejected. PEI samples with a 2 mm notch showed similar linear stress–strain behavior with different break stress and strain values. However, PEI/CF PEEK bimaterial showed deviation from linear curve and will be discussed in the following section.

Effect of notch size

In all cases, larger notches gave lower breaking stresses and breaking strains. Because the stress–strain behavior of monolithic CF PEEK and the PEI were more-or-less linear, it was possible to construct linear plots of breaking stress versus the inverse half power of the notch size ($a^{-1/2}$), shown in Figure 5. The points are experimental data. The solid lines represent linear regression that has been forced to pass through the origin. Using the slope of these lines and the tensile moduli of unnotched samples in conjunction with eq. (18), fracture energies were determined to be $G^{**} = 2$ kJ/m^2 for monolithic CF PEEK and the $G^{**} = 3.6$ kJ/m^2 for PEI. The PEI/CF PEEK data showed more complicated trend and linear regression did not give a good result.

The PEI/CF PEEK data also were analyzed using a more general approach. Strain energy densities were determined by integrating stress–strain curves up to the point of crack initiation, eq. (16), and then computing fracture energies, G, with eq. (15). Figure 6 shows G values for PEI/CF PEEK with various notch lengths. Fracture energies are summarized in Table III for the materials of construction as well as their series composite. The differences among G, G^*, and G^{**} are due to the nonlinearity of the stress–strain curves. G values for monolithic PEI and CF PEEK were in general agreement with values reported by other investigators.[26–29] PEI/CF PEEK bimaterial composites were not as tough as monolithic PEI specimens, but showed greater toughness than amorphous commodity polymers such as PS.[30]

The larger variation observed in the breaking stresses, breaking strains, and fracture energies of the composite samples probably arose from a variety of sources: variation in the shape of the interface, notch location relative to the interface, as well as sample handling and placement. (The standard devi-

TABLE II
Tensile Properties of the Materials of Construction and Bimaterial Composites (unnotched, $\lambda_1 = \lambda_2 = 0.5$, $T = 23°C$, $v = 2$ mm/min)

Materials	σ_y (MPa)	ε_y (m/m)	σ_b (MPa)	ε_b (m/m)	E (GPa)
PEI	103 ± 1	0.071 ± 0.001	101 ± 2	0.78 ± 0.07	3.2 ± 0.1
CF PEEK	NY	NY	129 ± 1	0.018 ± 0.001	12.0 ± 0.4
PEI/CF PEEK	NY	NY	60 ± 5	0.014 ± 0.001	4.9 ± 0.2

NY, no yield.

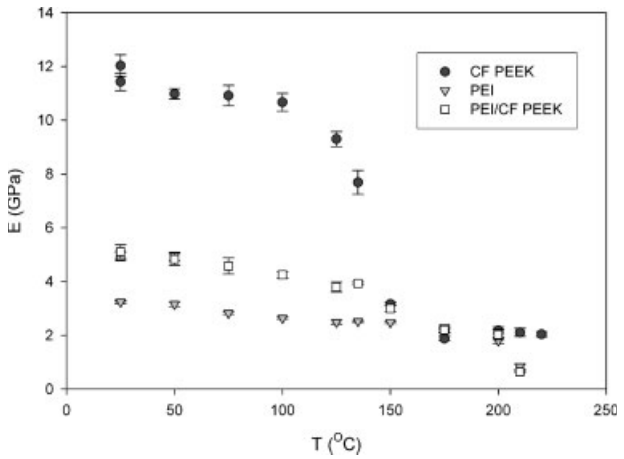

Figure 3 Modulus, E, versus temperature, T, for PEI, CF PEEK, and PEI/CF PEEK bimaterial composites ($\lambda_1 = \lambda_2 = 0.5$, $T = 23°C$, $v = 2$ mm/min).

ation for the unnotched PEI/CF PEEK also was considerably larger than the unnotched monolithic specimens, Table II.)

Rate dependence of fracture energies

Monolithic and composite specimens with 2 mm notches were pulled at strain rates ranging from 1.5×10^{-4} s^{-1} to 7.3×10^{-2} s^{-1} (v = 1–500 mm/min) to uncover any potential rate effects. Figure 7 shows fracture energy versus strain rate. No rate dependence was observed for the strain rates examined.

Temperature dependence of fracture energies

Fracture energies also were measured at various temperatures. Results are shown in Figure 8. With increases in temperature, G values for PEI increased slightly and decreased after around 125°C. The G values for CF PEEK and PEI/CF PEEK remained almost the same until the T_g of PEEK and decreased beyond the T_g.

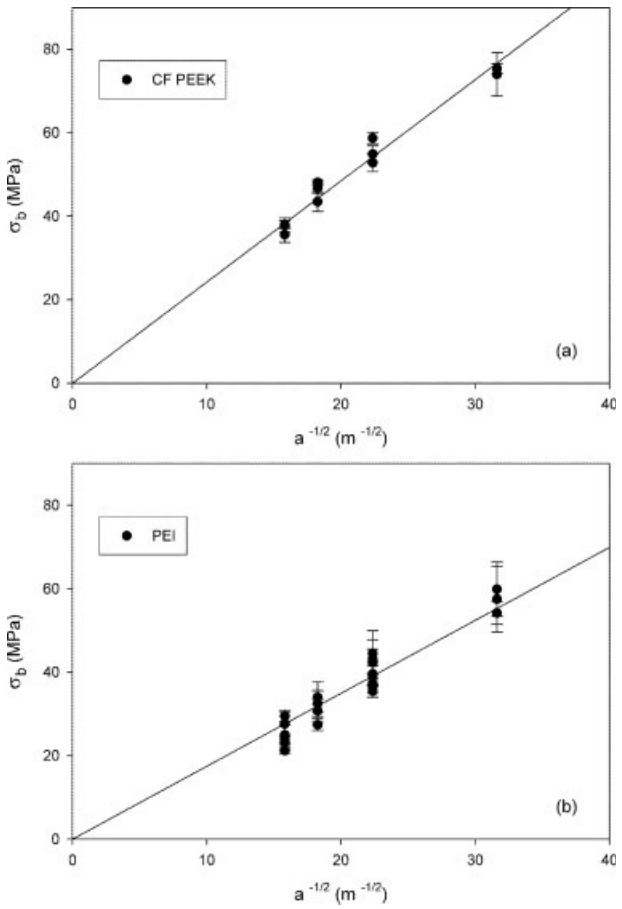

Figure 5 Breaking stress, σ_b, as a function of notch size, a, (a) for monolithic CF PEEK and (b) for monolithic PEI ($T = 23°C$, $v = 2$ mm/min).

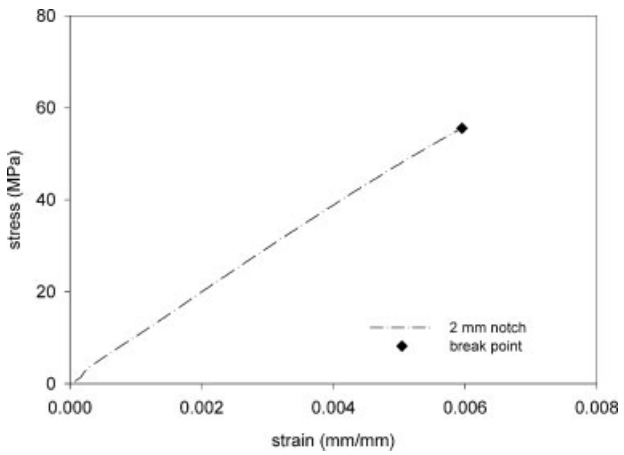

Figure 4 Stress versus strain for CF PEEK with a 2 mm notch ($T = 23°C$, $v = 2$ mm/min).

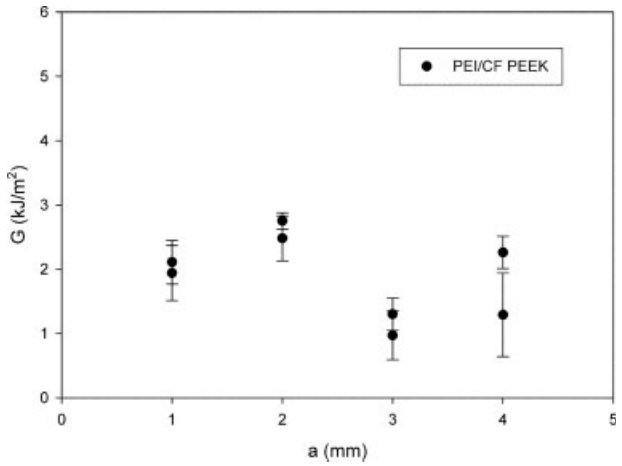

Figure 6 Fracture energy, G, versus notch size, a, for PEI/CF PEEK bimaterials ($T = 23°C$, $v = 2$ mm/min).

TABLE III
Fracture Energies of the Materials of Construction and Bimaterial Composites
($\lambda_1 = \lambda_2 = 0.5$, $T = 23^\circ$C, $v = 2$ mm/min)

Material	G (kJ/m^2)	G^* (kJ/m^2)	G^{**} (kJ/m^2)
PEI	4.5 ± 0.9	4.3 ± 0.4	3.6 ± 0.7
CF PEEK	2.8 ± 0.3	2.6 ± 0.3	2.0 ± 0.2
PEI/CF PEEK	1.9 ± 0.3	1.8 ± 0.2	1.5 ± 0.3
PC/CF PEEK	1.6 ± 0.6	NM	1.2 ± 0.5
PS	1.4 ± 0.3	NM	1.2 ± 0.2

NM, not measured. Data for PC/CF PEEK and PS were taken from Ref. 6.

Interface analysis

Microscopy

PEI/CF PEEK samples showed crack propagation in the immediate vicinity of the interface due to high associated stresses.[31–35] Fracture apparently occurred in a cohesive fashion with the crack propagating through the CF PEEK in close proximity to the interface, leaving a thin layer of CF PEEK on the PEI. Turned on end, the fracture surfaces of the PEI and CF PEEK segments were indistinguishable—both resembled CF PEEK. Figure 9 shows the OM images of an unnotched PEI/CF PEEK fracture interface. Images are from the more transparent PEI side. The top picture represents the whole cross section of sample and the bottom picture is a more highly magnified view of the center region. Higher magnification showed that the fracture surfaces were covered with clusters of carbon fiber surrounded by fiber-free areas. Fiber-free areas had the yellowish cast of PEI. Thus, from OM alone, it was not clear if these fiber-free regions were completely covered by PEEK or not.

Figure 10 shows the SEM images of the PEI/CF PEEK interface from PEI side. Although OM revealed fiber-free areas, impressions left by carbon fiber were evident everywhere on the fracture surface, an additional indicator that failure likely occurred inside the CF PEEK.

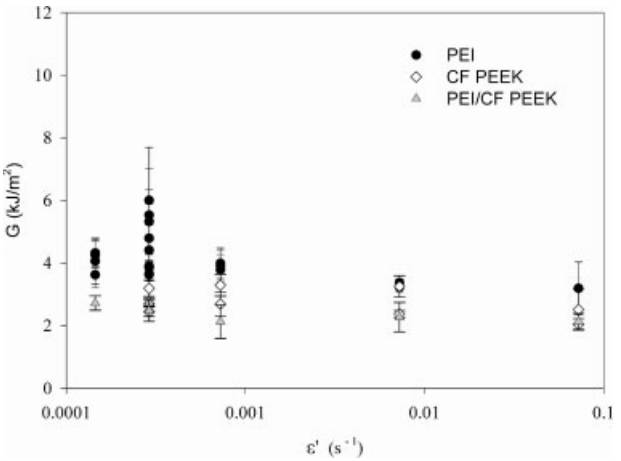

Figure 7 Fracture energy, G, versus strain rate, ε', for PEI, CF PEEK, and PEI/CF PEEK bimaterials ($T = 23^\circ$C).

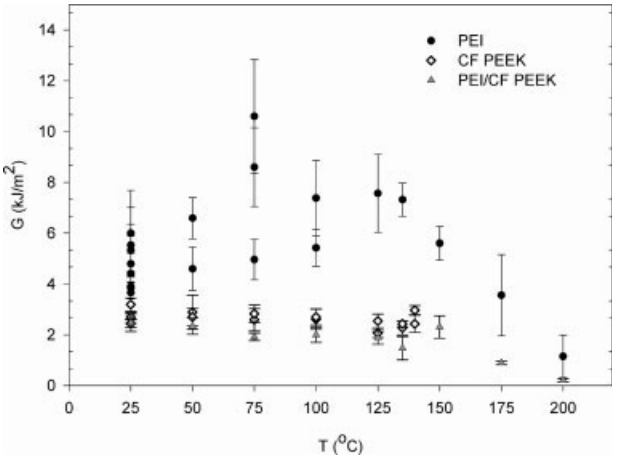

Figure 8 Fracture energy, G, versus temperature, T, for PEI, CF PEEK, and PEI/CF PEEK bimaterials ($v = 2$ mm/min).

XPS spectra from the fracture surfaces

Figure 11 shows the XPS spectra from the PEI/CF PEEK fracture surface. From the microscopy analysis, the failure was believed to occur mostly inside the CF PEEK layer. XPS analysis confirmed this. Nitrogen exists in PEI, but not in PEEK. The PEI side showed no

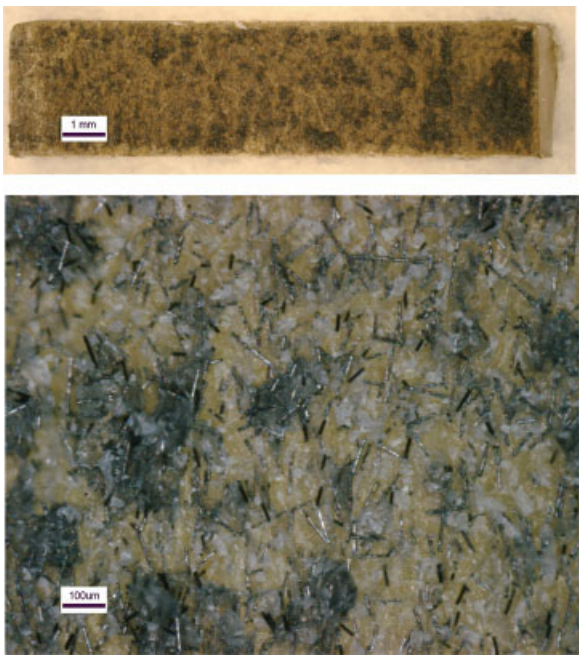

Figure 9 Optical microscopy pictures of the fracture surfaces of an unnotched PEI/CF PEEK bimaterial composite (PEI side). The two images have different magnifications. The top image has a magnification of 10×; the bottom one has 100×. [Color figure can be viewed in the online issue, which is available at www.interscience.wiley.com.]

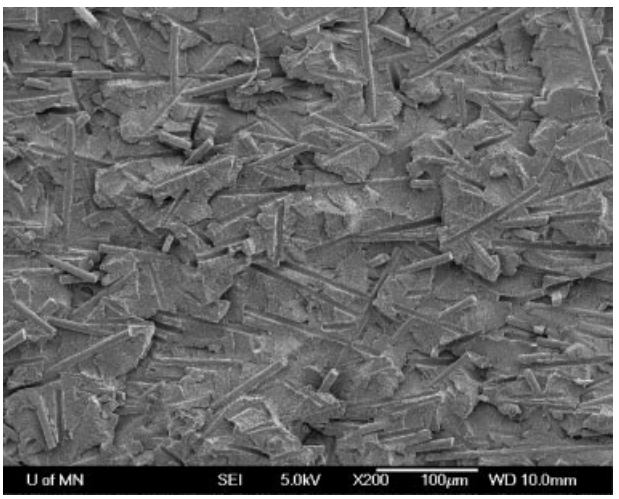

Figure 10 SEM photographs of an unnotched PEI/CF PEEK bimaterial composite fracture surface (PEI side).

evidence of nitrogen. The XPS spectra from the two fracture surfaces were identical. Both showed the characteristic peaks associated with PEEK, substantiating that the PEI side was indeed covered by thin layer of PEEK. Refer to the Appendix for more information regarding the XPS spectra of PEI and PEEK.

The combination of the good interfacial adhesion, carbon fibers acting as stress initiators, and the lower yield stress of PEEK matrix[23] compared to PEI probably led to failure through the CF PEEK.

Comparison to PC/CF PEEK from earlier studies

Compared to PC/CF PEEK bimaterial composites evaluated in earlier studies,[6] the PEI/CF PEEK specimens examined here showed higher modulus (+25%), higher breaking stress (+67%), and a greater fracture energy (+20%). The improvement in breaking stress of the PEI composites relative to the PC composites is greater than that expected from increased stiffness alone. PEI is miscible with PEEK whereas PC is not. The miscibility between PEI and PEEK led to a stronger interfacial bond. The cohesive fracture of the PEI/CF PEEK was rather uniform and left a thin layer of CF PEEK on the PEI. In contrast, the fracture of PC/CF PEEK composites was adhesive in nature with interfacial failure in the center of the specimen and fragments of PC attached to the edge of CF PEEK.

CONCLUSIONS

Bimaterial composites were constructed by injecting CF PEEK into a mold containing one-half of a PEI specimen. Specimens were notched and tested in tension. Using fracture mechanics, the adhesion strength of the interfaces (a fracture energy with units of energy per area) was calculated from notch size and stress–strain behavior of the notched specimens. Fracture energies of the composites were less than the materials of construction, yet indicated a strong adhesive bond. Variations in test speed had little effect on fracture energy. Fracture energies, however, did decline slightly with increasing temperature.

All specimens broke in the general vicinity of the bimaterial interface. Microscopy and XPS confirmed cohesive fracture through the CF PEEK, leaving a thin layer of CF PEEK on the PEI. The excellent adhesive strength exhibited by the PEI/CF PEEK was attributed in part to the miscibility of PEI and PEEK. The strength of the adhesive bond of PEI/CF PEEK

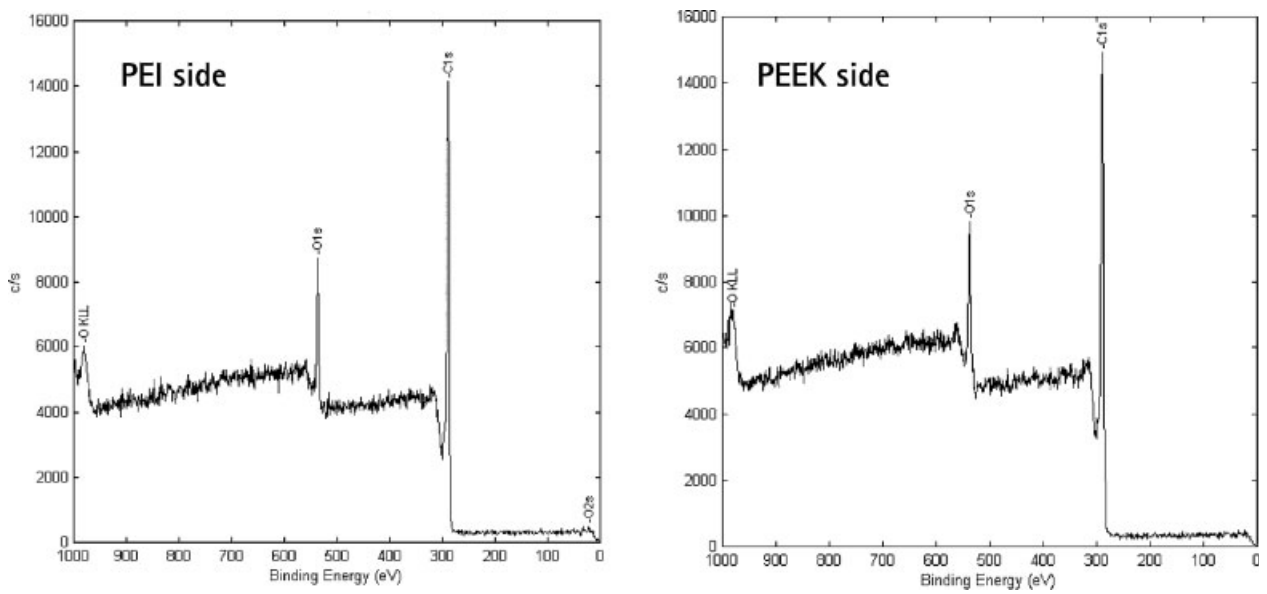

Figure 11 XPS spectra of the fracture surfaces of a PEI/CF PEEK composite.

composites is greater than the cohesive strength of amorphous commodity polymers such as PS.

APPENDIX: X-RAY PHOTOELECTRON SPECTRA OF PEI AND PEEK

Figure A1 shows the chemical structure and XPS spectra of PEI and PEEK. PEI has carbon, oxygen, nitrogen, and hydrogen in its structure. (Hydrogen is not detected by XPS.) The elemental ratio from the XPS spectrum is in good agreement with the ratio from the chemical structure. From the magnified image of C_{1s} region, detailed information on the oxidation state of carbon atom can be obtained. The C_{1s} peak at 285 eV is dominated by carbon that is bonded to other carbon atoms. Carbon in the imide group has a higher oxidation state and manifests itself as a small shoulder peak at 288.3 eV. In the case of O_{1s} peak, oxygen from imide group and ether group had only slightly different binding energies. Clear separation of these two peaks

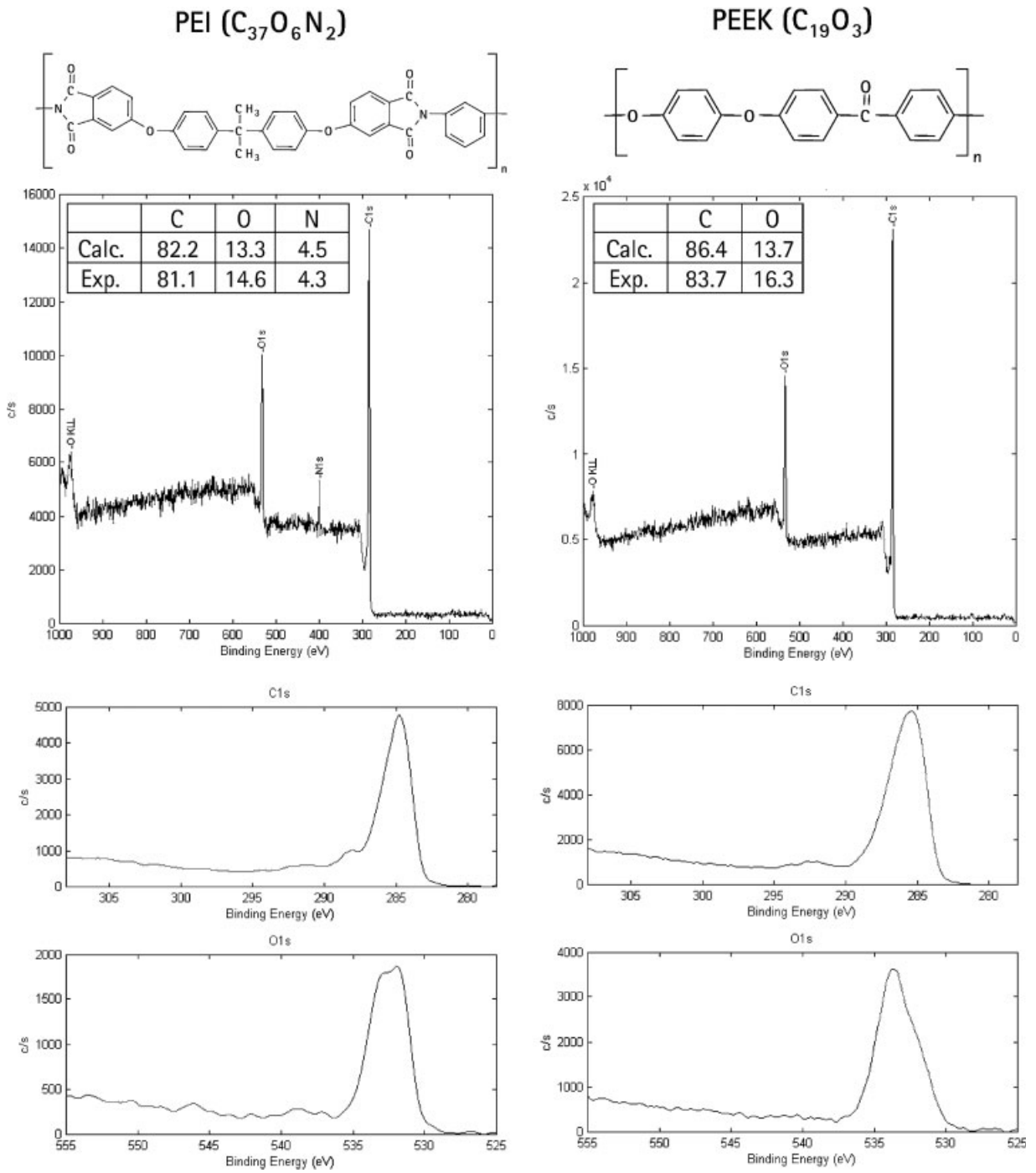

Figure A1 XPS spectra of monolithic PEI and PEEK surfaces.

that reside near 532–533 eV is quite difficult. That said, the ratio of ether-to-imide oxygen is 1–2 for PEI. O_{1s} showed an asymmetric peak according to this oxygen ratio. On the other hand, nitrogen showed a distinct peak at 400 eV.

PEEK contains only carbon, oxygen, and hydrogen. The carbon atoms in PEEK can be separated into three groups. The carbon atoms in the aromatic ring that are attached only to other carbon atoms showed a major peak at 285 eV. The carbon attached to oxygen and carbon in carbonyl group show peaks at slightly higher binding energy and make the whole C_{1s} peak look asymmetric. The aromatic ring of PEEK shows a very small shake-up peak at 292.5 eV. The difference between the oxygen in ether and carbonyl group in the O_{1s} peak also is small and showed one asymmetric peak near 532–533 eV. The shoulder at a lower binding energy (532 eV) belongs to the ketone groups of PEEK. In contrast to PEI, PEEK has more oxygen in the ether group.

References

1. Kausch, H. H. Advanced Thermoplastic Composites; Hanser: New York, 1993.
2. De Gaspari, J. Plast Technol 1998, 44, 44.
3. Bhatt, S. Micro 1999, 17, 37.
4. Extrand, C. W.; Bhatt, S. J Appl Polym Sci 2000, 76 1777.
5. Extrand, C. W.; Bhatt, S. J Adhes 2000, 72, 219.
6. Extrand, C. W.; Bhatt, S. J Mater Sci 2000, 35, 5427.
7. Extrand, C. W.; Bhatt, S. J Appl Polym Sci 2000, 78, 173.
8. Saechtling, H. Plastics Handbook, 2nd ed.; Oxford University Press: New York, 1992.
9. Johnson, L. R., Ed. International Plastics Selector, Vol. 2; D.A.T.A. Business Publishing: Englewood, CO, 17th ed., 1996.
10. Brandrup, J.; Immergut, E. H.; Grulke, E. A., Eds. Polymer Handbook, 4th ed.; Wiley: New York, 1999.
11. Harris, J. E.; Robeson, L. M. J Polym Sci Part B: Polym Phys 1987, 25, 311.
12. Harris, J. E.; Robeson, L. M. J Appl Polym Sci 1988, 35, 1877.
13. Crevecoeur, G.; Groenickx, G. Macromolecules 1991, 24 1190.
14. Chen, H. L.; Porter, R. S. Polym Eng Sci 1992, 32, 1870.
15. Hsiao, B. S.; Sauer, B. B. J Polym Sci Part B: Polym Phys 1993, 31, 901.
16. Runt, J. P. In Encyclopedia of Polymer Science and Engineering, Vol. 4; Mark, H. F., Kroschwitz, J. I., Eds.; Wiley: New York, 2nd ed., 1986.
17. Blundell, D. J.; Osborn, B. N. Polymer 1993, 24, 953.
18. Ward, I. M. Mechanical Properties of Solid Polymers, 2nd ed.; Wiley: New York, 1983.
19. Gere, J. M.; Timoshenko, S. P. Mechanics of Materials, 2nd ed.; PWS-Kent: Boston, 1984.
20. Griffith, A. A. Philos Trans R Soc London Ser A 1920, 211, 163.
21. Williams, J. G. Fracture Mechanics of Polymers; Wiley: New York, 1987.
22. Cebe, P.; Chung, S. Y.; Hong, S.-D. J Appl Polym Sci 1987, 33, 487.
23. Gensler, R.; Béguelin, P. H.; Plummer, C. J. G.; Kausch, H.-H.; Munstedt, H. Polym Bull 1996, 37, 111.
24. Albérola, N. D.; Mélé, P.; Bas, C. J Appl Polym Sci 1997, 64, 1053.
25. Extrand, C. W.; Bhatt, S.; Monson, L. J Mater Sci 2001, 36, 4603.
26. Hine, P. J.; Brew, B.; Duckett, R. A.; Ward, I. M. Compos Sci Technol 1988, 33, 35.
27. Hashemi, S.; Kinloch, A. J.; Williams, J. G. J Compos Mater 1990, 24, 918.
28. Blackman, B. R. K.; Dear, J. P.; Kinloch, A. J.; MacGillivray, H.; Wang, Y.; Williams, J. G.; Yayla, P. J Mater Sci 1995, 30, 5885.
29. Kim, A.; Bosnyak, C. P.; Chudnovsky, A. J Appl Polym Sci 1994, 51, 1841.
30. Wu, S. Polymer Interface and Adhesion; Marcel Dekker: New York, 1982.
31. Williams, M. L. Bull Seismol Soc Am 1959, 49, 199.
32. Sih, G. C.; Rice, J. R. J Appl Mech 1964, 31, 477.
33. Erdogan, F. J Appl Mech 1965, 32, 403.
34. Rice, J. R.; Sih, G. C. J Appl Mech 1965, 32, 418.
35. Hein, V. L.; Erdogan, F. Int J Fract Mech 1971, 7, 317.